

Crystal and electronic structures of BiS₂-based compounds Sr_{0.5}X_{0.5}FBiS₂ (X = rare earth) under pressure: Correlation with the change in the superconductivity from unconventional to conventional

Hitoshi Yamaoka ^{1,*} Aichi Yamashita ² Yuki Nakahira ² Masayuki Ochi ^{3,4} Kazuhiko Kuroki,³ Hiroto Arima ^{2,5} Kazuyuki Matsubayashi ⁵ Hirofumi Ishii,⁶ Nozomu Hiraoka ⁶ and Yoshikazu Mizuguchi ^{2,†}

¹RIKEN SPring-8 Center, Sayo, Hyogo 679-5148, Japan

²Department of Physics, Tokyo Metropolitan University, 1-1 Minami-Osawa, Hachioji 192-0397, Japan

³Department of Physics, Osaka University, Machikaneyama-cho, Toyonaka, Osaka 560-0043, Japan

⁴Forefront Research Center, Osaka University, Machikaneyama-cho, Toyonaka, Osaka 560-0043, Japan

⁵Department of Engineering Science, The University of Electro-Communications, Chofu 182-8585, Tokyo, Japan

⁶National Synchrotron Radiation Research Center, Hsinchu 30076, Taiwan

 (Received 6 June 2022; revised 7 September 2022; accepted 18 October 2022; published 14 November 2022)

Sr_{1-x}X_xFBiS₂ (X: rare earth) is considered to show a pressure-induced structural transition around 1 GPa where the superconductivity changes from unconventional in the low-pressure phase to conventional in the high-pressure phase with increasing the superconducting transition temperature (T_c). We clarified the monoclinic crystal structure ($P2_1/m$) in the high-pressure phase which is the same as the high-pressure phase of $XO_{1-x}F_xBiY_2$ (Y: chalcogen) systems. We performed high-resolution x-ray absorption spectroscopy (XAS) to study the electronic structure of Sr_{1-x}X_xFBiS₂ systematically, indicating the Bi charge state of nearly 3+. The pressure dependence of the XAS spectra of Sr_{0.5}La_{0.5}FBiS₂ and Sr_{0.5}Nd_{0.5}FBiS₂ indicate a large change in the electronic structure around the structural transition pressure, which corresponded to the transition from semiconductorlike to more metallic states. The increase of the empty states of Bi *s* and *d* (t_{2g}) bands above the Fermi level was observed in the high-pressure phase. Density functional theory calculations showed that the density of the states at the Fermi level did not show a significant change in the high-pressure phase, where higher T_c was observed.

DOI: [10.1103/PhysRevB.106.205122](https://doi.org/10.1103/PhysRevB.106.205122)

I. INTRODUCTION

A new family of layered superconductors of BiS₂-based compound, Bi₄O₄S₃, with the superconducting transition temperature $T_c = 8.6$ K was discovered in 2012 [1–4]. The crystal structure consists of alternate stacks of a BiS₂ superconducting layer and an insulating (blocking) layer [5,6]. The alternate stacking structure in the BiS₂-based superconductors is similar to those in the Cu-oxide and Fe-based superconductors. Therefore the BiS₂-based superconductors have attracted many interests and many BiS₂-based superconductors have been synthesized mainly by replacing the blocking layer with other materials [7–9]. Pressure also affects the physical property with the appearance of the superconductivity in the BiS₂-based superconductors [10–12].

It was found that in $XO_{1-x}F_xBiY_2$ (X: rare earth, Y: chalcogen), the superconducting transition temperature (T_c) dramatically increased from a few Kelvin at ambient pressure to approximately 10 K under pressure [13–16]. The transition to higher T_c was triggered by a structural transition from tetragonal ($P4/nmm$) to monoclinic ($P2_1/m$) at around 1 GPa. The increase of T_c has been considered to be caused by an enhancement of two-dimensionality of the superconducting layer [16].

By replacing the LaO layer with the SrF block, a new class of BiS₂-based superconductors Sr_{1-x}X_xFBiS₂ (X = La, Ce) has been found [17–19]. In Sr_{0.5}La_{0.5}FBiS₂, fivefold increase of T_c above 1 GPa was observed accompanying the transition from the semiconductor to metallic states. Recently, a systematic study of the chemical and hydrostatic pressure effect for Sr_{0.5}X_{0.5}FBiS₂ (X = La, Ce, Pr, Nd, Sm) has been performed [20]. In these samples the shielding volume fraction of the superconductivity was estimated to be less than 6% at ambient pressure, indicating that the superconductivity was filamentary. Thus the chemical pressure with substituting smaller X such as Nd and Sm was not sufficient to induce bulk superconductivity in the Sr_{1-x}X_xFBiS₂ system. While the bulk superconductivity with the shielding volume SC fraction of nearly 100% was observed in the high-pressure phase after the structural transition around 1 GPa [20]. It has been known that the isotope effects on superconducting transition temperatures is a useful method to examine the pairing mechanism of the electron-phonon interaction. The isotope effects using ³²S and ³⁴S in the high-pressure phase of (Sr,La)FBiS₂ with a monoclinic crystal structure and a higher T_c of ~10 K under high pressures showed a conventional-type isotope shift in T_c [21]. Although the T_c of the low-pressure phase is too low to investigate isotope effects in Sr_{1-x}X_xFBiS₂, we could assume that the low-pressure (tetragonal) phase is an unconventional superconductor because of the observation of the absence of isotope effect in tetragonal in La(O,F)BiS₂ [22] and Bi₄O₄S₃ [23] at ambient pressure. In the tetragonal crystal structure,

*Corresponding author: yamaoka@spring8.or.jp

†Corresponding author: mizugu@tmu.ac.jp

the Bi p orbitals degenerate and a weak orbital-fluctuation mediated superconductivity through anharmonic lattice vibration was considered to be a candidate of the unconventional superconductivity [5,24–26]. Thus the superconductivity of $\text{Sr}_{1-x}\text{X}_x\text{FBiS}_2$ is considered to be changed from unconventional to conventional under pressure with increasing T_c . Therefore $\text{Sr}_{1-x}\text{X}_x\text{FBiS}_2$ system may be a good system to study the mechanism of the emergence of superconductivity in layered superconductors.

The mechanism to obtain the higher- T_c superconductors, however, has still not been fully understood in BiS_2 -based superconductors [5,6]. Change in the electronic structure induced by the chemical pressure or the hydrostatic pressure may be physically an important role in the emergency of the higher- T_c superconductivity [27]. In $\text{Sr}_{1-x}\text{X}_x\text{FBiS}_2$, however, no systematic study of the electronic structure under pressure has been performed as well as the chemical pressure effect on the electronic structure so far.

The purpose of this study is to clarify the electronic structures of $\text{Sr}_{1-x}\text{X}_x\text{FBiS}_2$ systematically and find the correlation between the change in the electronic structure and the emergence of the superconductivity as a function of chemical composition or hydrostatic pressure. We additionally prepared a (Sr,Nd)FBiSse sample for comparison. We measured the chemical composition (x) and pressure dependences of the high-resolution x-ray absorption spectra with partial fluorescence yield mode (PFY-XAS) at the Bi- L_3 and Se- K absorption edges, which has an advantage of the high-resolution measurements of the spectra by reducing the lifetime line broadening [28–32]. We found that a difference of the Bi- L_3 absorption edge for $X = \text{Nd}$ in $\text{Sr}_{1-x}\text{X}_x\text{FBiS}_2$ which may suggest a larger pseudogap and correlate to the higher transition pressure of the $X = \text{Nd}$ sample. The electronic structure in $\text{Sr}_{0.5}\text{X}_{0.5}\text{FBiS}_2$ ($X = \text{La}, \text{Nd}$) largely changed above the structural transition pressure. We measured x-ray diffraction patterns (XRD) patterns of $\text{Sr}_{0.5}\text{La}_{0.5}\text{FBiS}_2$ under pressure and clarified the monoclinic crystal structure at the high-pressure phase. Note that the XRD patterns in the high-pressure phase have been measured previously and the structural phase transition from the tetragonal to monoclinic crystal structure was suggested [20]. However, exact analyses for the high-pressure phase have not yet been completed. Furthermore, we performed density functional theory (DFT) calculations at the low-pressure tetragonal and high-pressure monoclinic crystal structures. Surprisingly, no rapid increase of the density of states (DOS) at the Fermi level (E_F) was suggested at the high-pressure phase where the bulk superconductivity occurs.

II. METHODS

A. Experiments

Polycrystalline samples of (Sr, X)FBiS₂ ($X = \text{La}, \text{Ce}, \text{Pr},$ and Nd) and (Sr,Nd)FBiSse were prepared by a solid-state reaction method in an evacuated quartz tube [10,20]. Powders of X_2S_3 ($X: \text{La}$ (99.9%), Ce (99.9%), Pr (99%), Nd (99%), and Sm (99.9%)), SrF_2 (99%), Bi (99.999%), and S (99.9999%) were weighed for $\text{Sr}_{0.5}\text{X}_{0.5}\text{FBiS}_2$ and $\text{Sr}_{0.74}\text{Nd}_{0.26}\text{FBiSse}$. They were mixed with powders with a nominal composition

of $\text{Sr}_{0.5}\text{X}_{0.5}\text{FBiS}_2$ in an Ar-filled glove box. The mixed powder was pelletized, and sintered in an evacuated quartz tube at 700 °C for 20 hours, followed by furnace cooling to room temperature. The obtained compounds were thoroughly mixed, ground, and sintered under the same conditions as the first sintering.

Electrical resistivity of $\text{Sr}_{0.5}\text{La}_{0.5}\text{FBiS}_2$ was measured up to 6.5 GPa using an opposite anvil cell [33]. The culet size of the tungsten carbide anvil was 3 mm in diameter with a gasket of nonmagnetic Ni-Cr-Al alloy. A pressure medium of glycerin was used. We used T_c of Pb as a pressure gauge.

Pressure dependence of the XRD patterns for the powder sample of $\text{Sr}_{0.5}\text{La}_{0.5}\text{FBiS}_2$ was measured at SPring-8 BL12B2 using a three-pin plate DAC (Almax Industries) with a CCD detection system at room temperature. The culet size of the diamond anvil was 0.4 mm with a stainless steel gasket. We took an arrangement of both incoming and outgoing x-ray beams passed through the diamonds with an incident photon energy of 18 keV. Daphne 7474 oil was loaded as the pressure medium. 2D image of CCD was integrated by using FIT2D program [34]. The diffraction patterns were analyzed by the Rietveld method using the RIETAN-FP program [35,36]. The schematic images of crystal structures were drawn by VESTA [37].

Measurements of the PFY-XAS spectra were performed at BL12XU, SPring-8 [31,38]. Johann-type spectrometers were equipped with a spherically bent Si(577) analyzer of radius of ~ 1 m for Se $K\beta_1$ emission and Si(555) for Bi $L\alpha_1$ emission with a Si solid-state detector (Amptech) [32,39]. In the measurements of the chemical composition dependence we set the sample holder vertical to the incident beam and the emissions from the samples are detected at an angle of 75° to the beam axis. At the emitted photon energy of 12.66 keV the overall energy resolution was set to be approximately 1.5 eV. It is noted that one can discuss the relative change in the energy on the order of 0.1 eV which is one order of magnitude smaller than the energy spread of the analyzer. The intensities of the measured spectra were normalized using the intensity of the incident beam that was monitored just before the sample. The errors in the intensity and energy of each component of the PFY-XAS spectrum originated mainly from the statistical errors of the total counts and the fit errors. The intensities of the PFY-XAS spectra are normalized by the areas in the measured-energy range.

For the high-pressure experiments in the x-ray emission spectroscopy the x-ray beam was focused to ~ 33 (horizontal) $\times \sim 13$ (vertical) μm^2 at the sample position using a toroidal and a Kirkpatrick-Baez mirror. In the high-pressure measurements the emissions are detected at 90° to the beam axis. High-pressure conditions were achieved using a diamond anvil cell coupled with a gas membrane. A Be-gasket of 3 mm in diameter and approximately 100 μm thick was preindented to approximately 40–50 μm thickness around the center. The diameter of the sample chamber in the gasket was approximately 120 μm and the diamond anvil culet size was 300 μm . A pressure medium of Daphne 7474 was used for the DAC. The pressure was monitored by the ruby fluorescence method [40–42]. All measurements here were performed at room temperature.

B. Theoretical calculations

We used the Perdew-Burke-Ernzerhof parametrization of the generalized gradient approximation (PBE-GGA) [43] and the projector augmented wave (PAW) method [44] as implemented in the Vienna *ab initio* simulation package [45–48]. The core electrons in the PAW potentials were taken as follows: [He] for F, [Ne] for S, [Ar]3*d*¹⁰ for Sr, [Kr]4*d*¹⁰ for La, and [Xe]5*d*¹⁰4*f*¹⁴ for Bi. The spin-orbit coupling was included. The plane-wave cutoff energy of 550 eV and a 10 × 10 × 4 *k* mesh were used. We used the lattice parameters and atomic coordinates determined by our experiments: 0-GPa and 1.51-GPa structures for the tetragonal and monoclinic phases, respectively. Virtual crystal approximation was applied to represent the 1 : 1 mixing of the La and Sr atoms. For calculating the density of states, we used a 24 × 24 × 10 *k* mesh.

III. RESULTS

A. Chemical composition dependence of the XAS spectra at ambient pressure

Figure 1(a) shows the PFY-XAS spectra of Sr_{0.5}La_{0.5}FBiS₂, Sr_{0.5}Ce_{0.5}FBiS₂, Sr_{0.5}Pr_{0.5}FBiS₂, Sr_{0.5}Nd_{0.5}FBiS₂ and Sr_{0.74}Nd_{0.26}FBiSSe with those of Bi, Bi₂Se₃, and Bi₂O₃ for comparison at the Bi-*L*₃ absorption edge. The intensity is normalized by the area. Figure 1(c) shows the energies at the Bi-*L*₃ absorption edge of Sr_{1-x}X_xFBiS₂ with those of Bi₂O₃ and Bi₂Se₃. The absorption edges of the Sr_{1-x}X_xFBiS₂ are near that of Bi₂O₃ as shown in Fig. 1(b), indicating the Bi charge state of nearly 3+. The absorption edge energy of Sr_{0.5}La_{0.5}FBiS₂ is relatively higher than other samples. Note that the transition pressures to the high-*T*_c phase of *X* = La, Ce, Pr, and Nd were measured to be 0.95, 1.15, 1.17, and 1.33 GPa, respectively [20]. The absorption edge may correlate to the Fermi level, and the above results may suggest a higher Fermi level of Sr_{0.5}Nd_{0.5}FBiSSe compared to the others and this result possibly connects to higher critical pressure to emerge the superconductivity.

Figure 1(d) shows the PFY-XAS spectra of Sr_{0.74}Nd_{0.26}FBiSSe, SeO₂, and Bi₂Se₃ at the Se-*K* absorption edge. From the analogy to the spectra of selenium compounds [49–53], the main peak attributes a 1*s*-4*p* dipole transition and Se 4*d* partial density of states hybridized with the Bi 6*s* and 6*p* states. Figure 1(e) indicates that Se 4*p* DOS of Sr_{0.74}Nd_{0.26}FBiSSe above the Fermi level is comparable to Bi₂Se₃.

B. *T*_c of Sr_{0.5}La_{0.5}FBiS₂ under pressure

Measurements of the electrical resistivity of Sr_{0.5}X_{0.5}FBiS₂ under pressure were limited up to the pressures of just above the structural phase transition [20]. Here, we measured the electrical resistivity of Sr_{0.5}La_{0.5}FBiS₂ up to 6.5 GPa as shown in Figs. 2(a) and 2(b). Temperature dependence of the electrical resistivity of Sr_{0.5}La_{0.5}FBiS₂ at 0 GPa shows a semiconductor-like behavior. The activation energy was estimated to be approximately 9.6 meV above 100 K at 0 GPa. Figure 2(c) shows *T*_c as a function of pressure with the data previously measured by magnetization [20]. *T*_c in

the monoclinic phase decreases gradually with pressure. This behavior of *T*_c in Sr_{0.5}La_{0.5}FBiS₂ is very similar to that in LaO_{1-x}F_xBiS₂ [15]. Figure 2(d) shows the electrical resistivity at 300 K and *T*_c^{onset} as a function of pressure. The semiconducting behavior in the tetragonal phase was suppressed in the monoclinic phase.

C. XRD under pressure

We measured the pressure dependence of the x-ray diffraction patterns of Sr_{0.5}La_{0.5}FBiS₂ powder sample. The XRD patterns from 0 to 1.35 GPa are shown in Fig. 3(a). In this study, we successfully fitted the XRD patterns in the high-pressure phase [54]. We note that the exact crystal structure in the high-pressure phase was not fully resolved before as described above [20]. We clarified the structural phase transition from tetragonal (*P*4/*nmm*) to monoclinic (*P*2₁/*m*) crystal structure approximately 1 GPa. Impurity phase was a space group of *P*3*c*₁ with LaF₃ type.

Pressure dependence of the lattice constants are shown in Figs. 3(c) and 3(d). Pressure-induced change in the *b* axis after the structural transition is small, while those in the *a* and *c* axis are remarkable. The *c* axis shows a sudden change at the pressure of the structural transition, indicating the first-order phase transition. The crystal has a layered structure stacking along the *c* axis. Pressure compress the crystal mainly along the *c* axis, distorting along the *a* axis and making the BiS₂ superconducting layers flat.

In Fig. 3(e), we show pressure dependence of the angle β, which is defined to be the angle between the *a* and *c* axes. The angle β increases linearly with pressure after the structural transition.

We also measured the XRD patterns of Sr_{0.5}Nd_{0.5}FBiS₂ under pressure and confirmed the monoclinic crystal structure in the high-pressure phase (see the Supplemental Material) [54]. In contrast to the case of Sr_{0.5}La_{0.5}FBiS₂, the pressure dependence of the lattice constant *c* and the volume of Sr_{0.5}Nd_{0.5}FBiS₂ change smoothly across the structural phase transition pressure. This may be caused by the coexistence of two phases around a wider pressure range from 0.97 to 2.39 GPa in Sr_{0.5}Nd_{0.5}FBiS₂.

The pressure dependence of the volume is shown in Fig. 3(f). In Fig. 3(f), we show a fit of the pressure-volume relation by using an empirical formula of the Murnaghan's equation of state, $\frac{V}{V_0} = [1 + p\frac{B'}{B_0}]^{-\frac{1}{B'}}$, where *p*, *V*, *V*₀, *B*₀, and *B*' are pressure, volume, volume at ambient pressure, bulk modulus of incompressibility, and its first derivative with respect to the pressure, respectively. We obtain the parameters of *B*₀ = 74.83 GPa, *B*' = 5.55, *V*₀ = 221.8 Å³ for Sr_{0.5}La_{0.5}FBiS₂ and *B*₀ = 47.66 GPa, *B*' = 5.08, *V*₀ = 223.2 Å³ for Sr_{0.5}Nd_{0.5}FBiS₂ [54].

Here, we introduce a parameter of in-plane chemical pressure to compare the effect of hydrostatic pressure on the BiY₂ plane with that of the chemical pressure in the tetragonal crystal structure [55]. We define the in-plane chemical pressure as (*R*_{Bi} + *R*_{Y1})/*D*_{Bi-Y1}, where *R*_{Bi}, *R*_{Y1}, and *D*_{Bi-Y1} are the ionic radii of Bi and Y1, and in-plane distance between Bi and Y1 in the Bi-Y1 plane, respectively. This is the same definition as the one introduced in Ref. [55]. Figure 3(g) shows the in-plane pressure as a function of the hydrostatic pressure. The

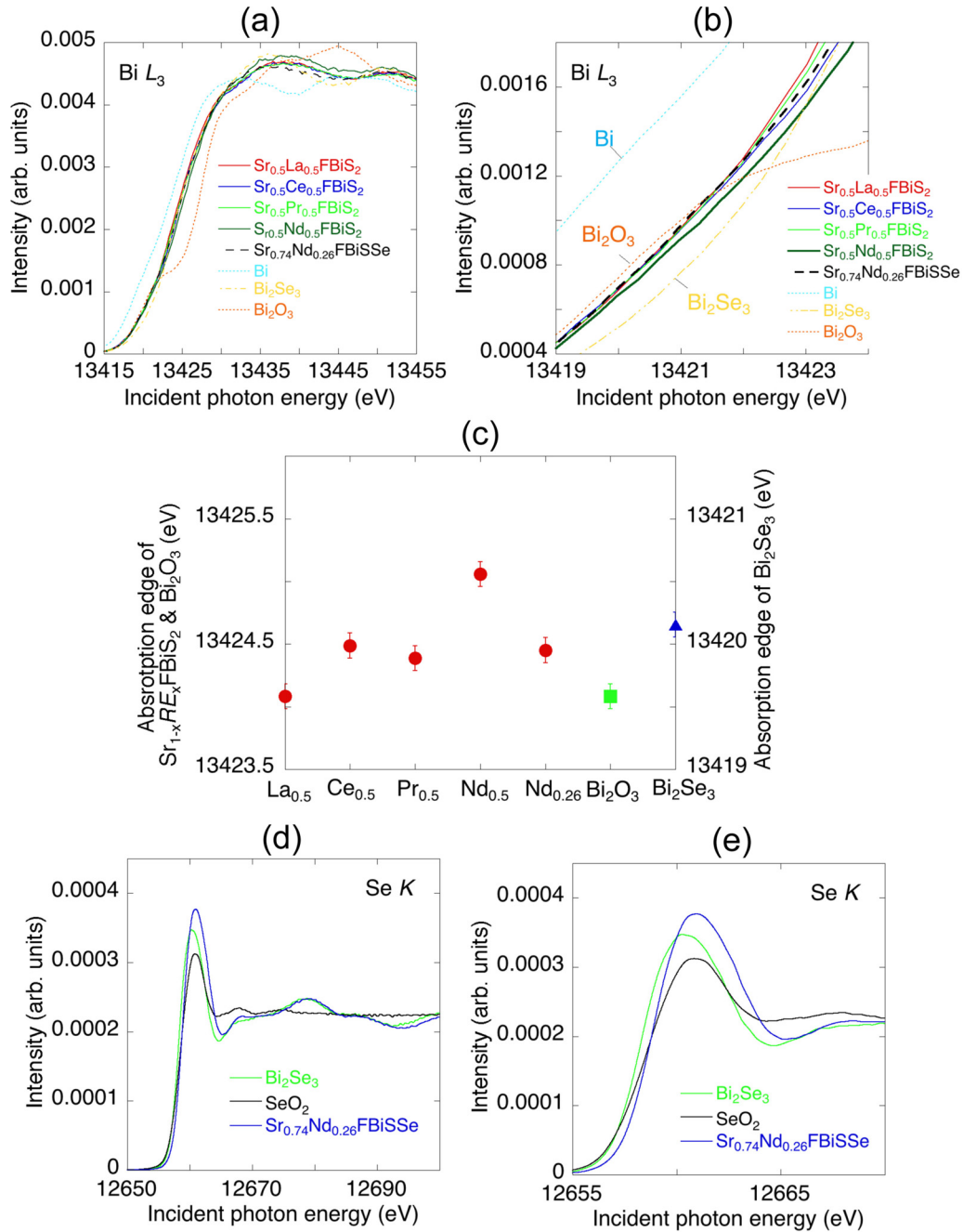


FIG. 1. (a) PFY-XAS spectra of $\text{Sr}_{1-x}\text{R}_x\text{FBiS}_2$ with those of Bi, Bi_2S_3 , and Bi_2O_3 at the Bi- L_3 absorption edge. The intensities are normalized by the areas. (b) Expanded view of (a) around the absorption edge. (c) Energies of the absorption edges estimated from the spectra in (a). (d) PFY-XAS spectra of $\text{Sr}_{0.74}\text{Nd}_{0.26}\text{FBiSe}$ with those of Bi_2S_3 and SeO_2 at the Se- K absorption edge. (e) Expanded view of (d) around the absorption edge.

in-plane pressure increases linearly in the tetragonal crystal structure, but the values are less than 1. Increase of T_c was observed in the in-plane pressure above 1.01 in $\text{XO}_{0.5}\text{F}_{0.5}\text{BiS}_2$ and $\text{LaO}_{0.5}\text{F}_{0.5}\text{BiS}_{2-x}\text{Se}_x$ [5]. Therefore it is considered that in $\text{Sr}_{0.5}\text{La}_{0.5}\text{FBiS}_2$ the structural transition occurs before reaching to the critical in-plane pressure in the tetragonal crystal structure phase.

Figure 3(h) shows the pressure dependence of the shielding volume fraction (SVF) of the superconductivity in the tetragonal crystal structure, where the data are taken from Ref. [20].

SVF increased with pressure and show a trend of rapid increase just before the structural transition pressure. Thus the bulk superconductivity may couple with the structural phase transition strongly.

D. XAS spectra under pressure

Figures 4(a)–4(d) show pressure dependence of the PFY-XAS spectra at the Bi- L_3 absorption edge of $\text{Sr}_{0.5}\text{La}_{0.5}\text{FBiS}_2$ and $\text{Sr}_{0.5}\text{Nd}_{0.5}\text{FBiS}_2$. In Fig. 4(e), we show a fit example of

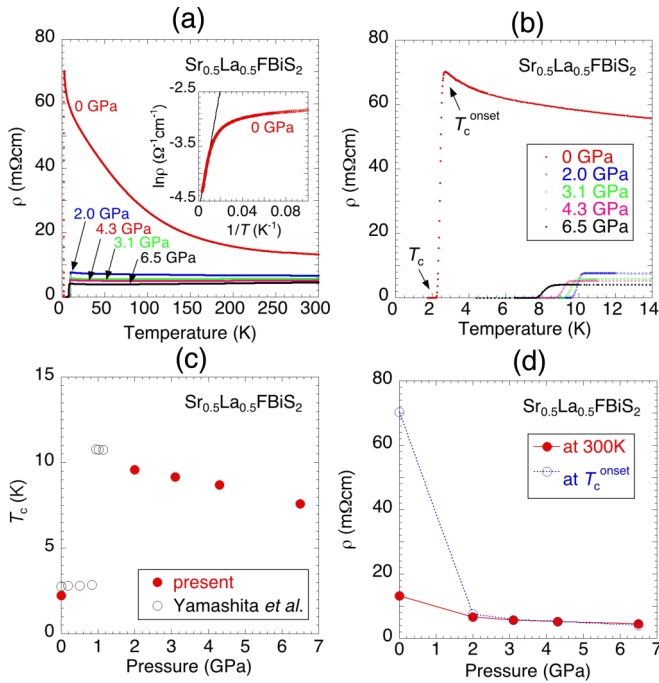


FIG. 2. (a) Temperature dependence of the electrical resistivity (ρ) of $\text{Sr}_{0.5}\text{La}_{0.5}\text{FBiS}_2$ under various pressures. An inserted figure shows a relation between $\ln\rho$ vs the inverse of the temperature at 0 GPa. A fit curve (solid line) to estimate the activation energy for the data at $T > 100$ K is also shown. (b) Expanded view of (a) around T_c . (c) T_c of $\text{Sr}_{0.5}\text{La}_{0.5}\text{FBiS}_2$ as a function of pressure (closed circles). Previously measured data are also shown (open circles) [20]. (d) The electrical resistance of $\text{Sr}_{0.5}\text{La}_{0.5}\text{FBiS}_2$ at 300 K and T_c^{onset} as a function of pressure.

the PFY-XAS spectrum at 0.41 GPa of $\text{Sr}_{0.5}\text{La}_{0.5}\text{FBiS}_2$ at the Bi- L_3 absorption edge. The spectra are fitted assuming some peaks of Voigt functions with an arctan-type background for simplicity. The peak A is assigned as a dipole-allowed transition of a $2p_{3/2}$ electron into $6s$ states [56–58]. A weak intensity of the peak A suggests that the Bi $6s$ state is not completely filled with electrons. Peaks B and C correspond to the transition of a $2p_{3/2}$ electron into $6d$ states of t_{2g} (B: non-bonding, $d_{xy,yz}$) and e_g (C: antibonding, d_{z^2}). Thus A reflects the Bi s DOS. D and C reflect the Bi d DOS above the Fermi level. The relative intensities of the peak A give the relative occupation probabilities of the $6s$ band in the ground state under the assumption that there is no hybridization between the Bi $6s$ and $6d$ orbitals [58].

Pressure-induced changes in the electronic structures of $\text{Sr}_{0.5}\text{Nd}_{0.5}\text{FBiS}_2$ is drastic around the pressure of the structural phase transition. On the other hand, that of $\text{Sr}_{0.5}\text{La}_{0.5}\text{FBiS}_2$ seems to change continuously. In both compounds, a rapid decrease of the energy of the Bi- L_3 absorption edge around the emergence of the superconductivity is observed as shown in Figs. 5(a)–5(d). The pressure dependence of the energy of the peak A (Bi $6s$ band) well corresponds to that of the Bi- L_3 absorption edge.

Figures 5(c)–5(h) show the fit results of the PFY-XAS spectra at the Bi- L_3 absorption edge for $\text{Sr}_{0.5}\text{La}_{0.5}\text{FBiS}_2$ and $\text{Sr}_{0.5}\text{Nd}_{0.5}\text{FBiS}_2$. The intensity of the peak A increases in

the superconducting region. The results indicate the pressure-induced increase of the empty states of the Bi $6s$ band. A similar phenomenon was also observed in Bi_2Se_3 [32]. In $\text{Sr}_{0.5}\text{Nd}_{0.5}\text{FBiS}_2$, the intensity of the peak B (Bi $6d$, t_{2g} band) increases in the superconducting region, and the energy of the peak B rapidly decreases at the pressure of the emergence of the superconductivity. On the other hand, in $\text{Sr}_{0.5}\text{La}_{0.5}\text{FBiS}_2$ the intensity of the peak B does not change through the pressure range of the structural phase transition although it shows an increase of around 7 GPa. The energy of the peak B in $\text{Sr}_{0.5}\text{La}_{0.5}\text{FBiS}_2$ gradually decreases with pressure similar to that of the peak A. The intensity of the peak C (Bi $6d$, e_g band) gradually decreases with pressure. The pressure-induced change in the electronic structure of $\text{Sr}_{0.5}\text{La}_{0.5}\text{FBiS}_2$ around 1 GPa is smaller than that of $\text{Sr}_{0.5}\text{Nd}_{0.5}\text{FBiS}_2$.

It is noted that we can fit the spectra without assuming the peak A component in the low-pressure range. The fits without the peak A show that the pressure dependencies of the peaks B and C do not change much because of very small intensity of the peak A [54]. On the other hand, the spectrum of $\text{Sr}_{0.5}\text{La}_{0.5}\text{FBiS}_2$ at 6.83 GPa and those of $\text{Sr}_{0.5}\text{Nd}_{0.5}\text{FBiS}_2$ at 3.2 and 5.26 GPa show an additional component of the peak A as shown in Figs. 4(b) and 4(d). This suggests the increase of the empty Bi $6s$ states, especially at high pressures, which may connect to the increase of the hybridization between Bi $6s$ and $6d$ orbitals.

The shift of the absorption edge to lower incident energy may suggest the shift of the Fermi level. Present XAS results explain the pressure-induced transition from the semiconductor-like to more metallic states observed in the temperature dependence of the electrical resistance in Fig. 2 and also in Ref. [20]. The increase of the empty states of the Bi s band above the Fermi level at the high-pressure phase may suggest the increase of the hybridization of the Bi $6s$ orbital with the p orbital [32,53]. While the monotonic decrease of the Bi d (e_g) band with pressure indicates the filling of the conduction electrons to the empty states.

After the structural phase transition around 1 GPa, the overall change in the electronic structure is not sensitive to pressure. This corresponds to the gradual change in T_c in the monoclinic phase as shown in Fig. 2(c).

E. Electronic structure calculations

We performed the DFT calculations for $\text{Sr}_{0.5}\text{La}_{0.5}\text{FBiS}_2$ in the tetragonal crystal structure at the low-pressure phase and the monoclinic crystal structure at the high-pressure phase using the experimental parameters measured. Figure 6 shows the band structures of the tetragonal and monoclinic crystal structures. The calculated results of $\text{Sr}_{0.5}\text{La}_{0.5}\text{FBiS}_2$ are similar to those of $\text{LaO}_{0.5}\text{F}_{0.5}\text{BiS}_2$ [59]. While the overall band structures are similar between the two crystal structures, the lowest conduction band at the $X(\pi/a, 0, 0)$ point in the monoclinic structure has two remarkable features; it exhibits a sizable band splitting (bilayer splitting) and is not equivalent to the $Y(0, \pi/b, 0)$ point. The band splitting is originated from the inter- BiS_2 layer coupling (bilayer coupling) strongly enhanced by the symmetry breaking of the crystal structure as observed in the monoclinic crystal structure of $\text{LaO}_{0.5}\text{F}_{0.5}\text{BiS}_2$ [59]. Thus, in the tetragonal crystal structure, the band

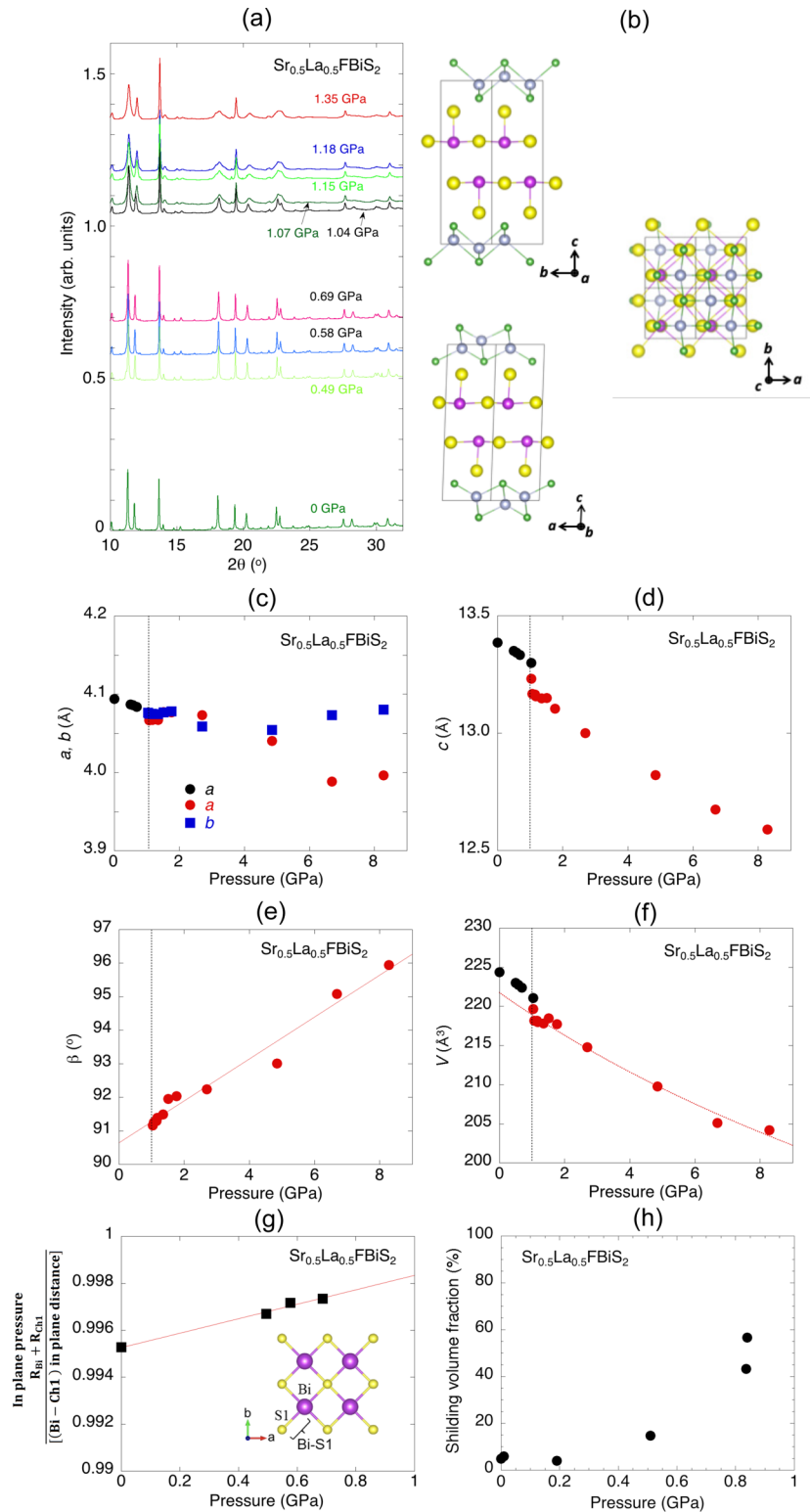


FIG. 3. (a) X-ray diffraction pattern of $\text{Sr}_{0.5}\text{La}_{0.5}\text{FBiS}_2$ in the pressure range from 0 to 1.35 GPa. Note that each baseline of the XRD patterns in the vertical scale is proportional to the pressure. (b) A schematic view of the monoclinic crystal structure in the high-pressure phase. (c) Pressure dependence of the lattice parameters along the a and b axes. (d) Pressure dependence of the lattice parameters along the c axis. (e) Pressure dependence of the angle between the a and c axes. A solid line is a linear fit. (f) Pressure dependence of the volume. A solid line is a fit in the high-pressure phase using an empirical formula of the Murnaghan's equation of state. In (c), (d), and (f), the errors are within the sizes of the symbols. (g) Hydrostatic pressure dependence of in-plane pressure in the tetragonal structure phase. (h) Pressure dependence of the shielding volume fraction of the superconductivity in the tetragonal crystal structure. They were estimated based on the results in Ref. [20].

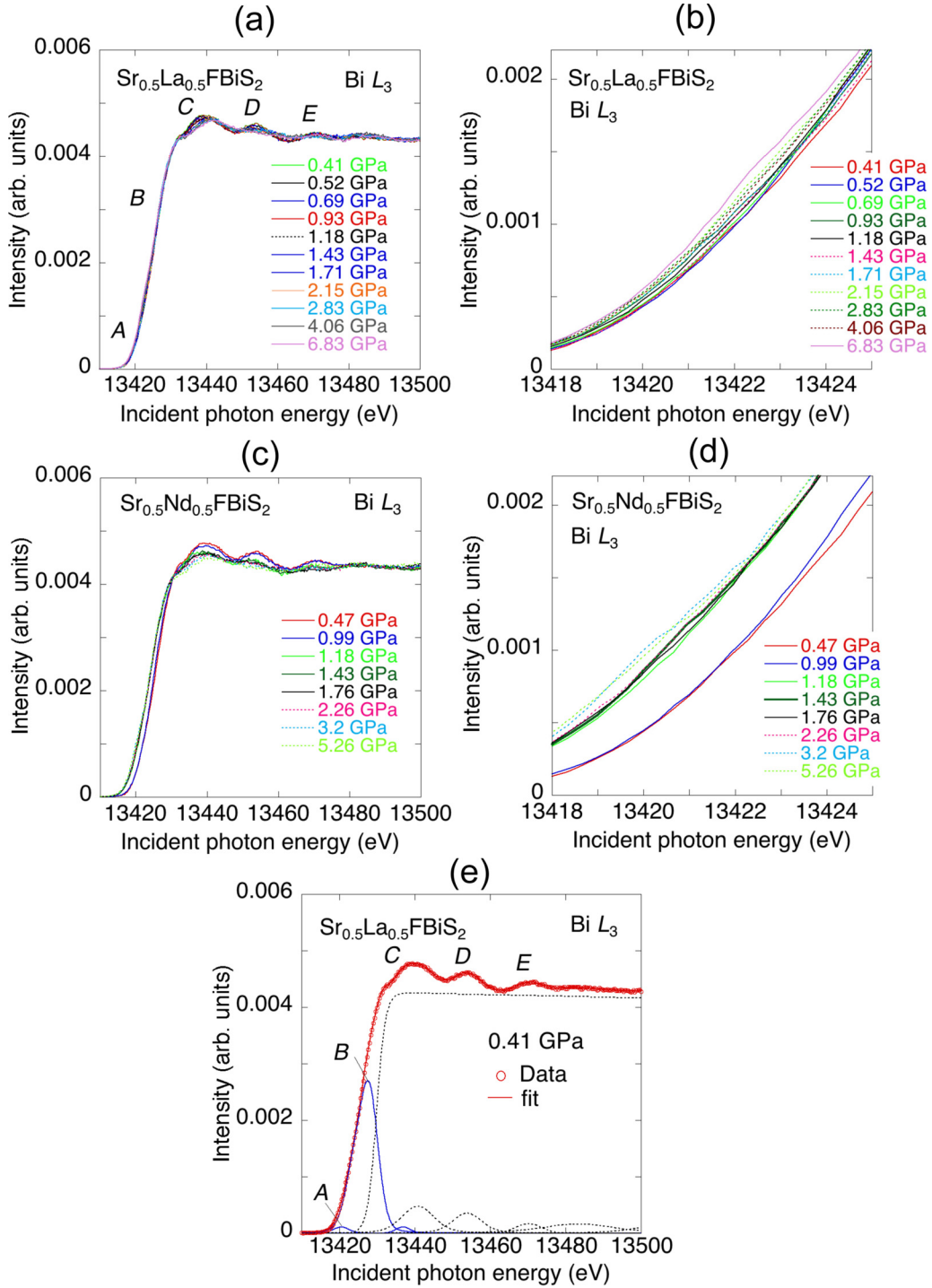


FIG. 4. (a) Pressure dependence of the PFY-XAS spectra of $\text{Sr}_{0.5}\text{La}_{0.5}\text{FBiS}_2$ at the Bi-L_3 absorption edge. (b) Expanded view of (a) around the absorption edge. (c) Pressure dependence of the PFY-XAS spectra of $\text{Sr}_{0.5}\text{Nd}_{0.5}\text{FBiS}_2$ at the Bi-L_3 absorption edge. (d) Expanded view of (c) around the absorption edge. (e) A fit example of the PFY-XAS spectrum at 0.41 GPa of $\text{Sr}_{0.5}\text{La}_{0.5}\text{FBiS}_2$ at the Bi-L_3 absorption edge.

splitting makes a nearly degenerate Fermi surface while in the monoclinic crystal structure much separated Fermi surface is observed due to the symmetry-broken monoclinic structure.

Figure 7 shows the total and partial DOS (pDOS) of the tetragonal and monoclinic crystal structures. Figures 7(a), 7(b), 7(d), and 7(e) suggest the hybridization of mainly $\text{Bi } 6p_x$

and $\text{Bi } 6p_y$, with $\text{S } 3p$ orbitals, constituting the Fermi surface [26,59,60]. DOS of these bands are larger than other orbitals and thus, the electron carriers are mainly in the BiS_2 layer. The $\text{Bi-}p$ pDOS and total DOS at E_F rather decreases in the monoclinic crystal structure as shown in Figs. 7(b) and 7(e). While Figs. 7(c) and 7(f) show that the $\text{Bi-}s$ and $\text{Bi-}d$ pDOS at E_F increase in the monoclinic crystal structure. The increase of the

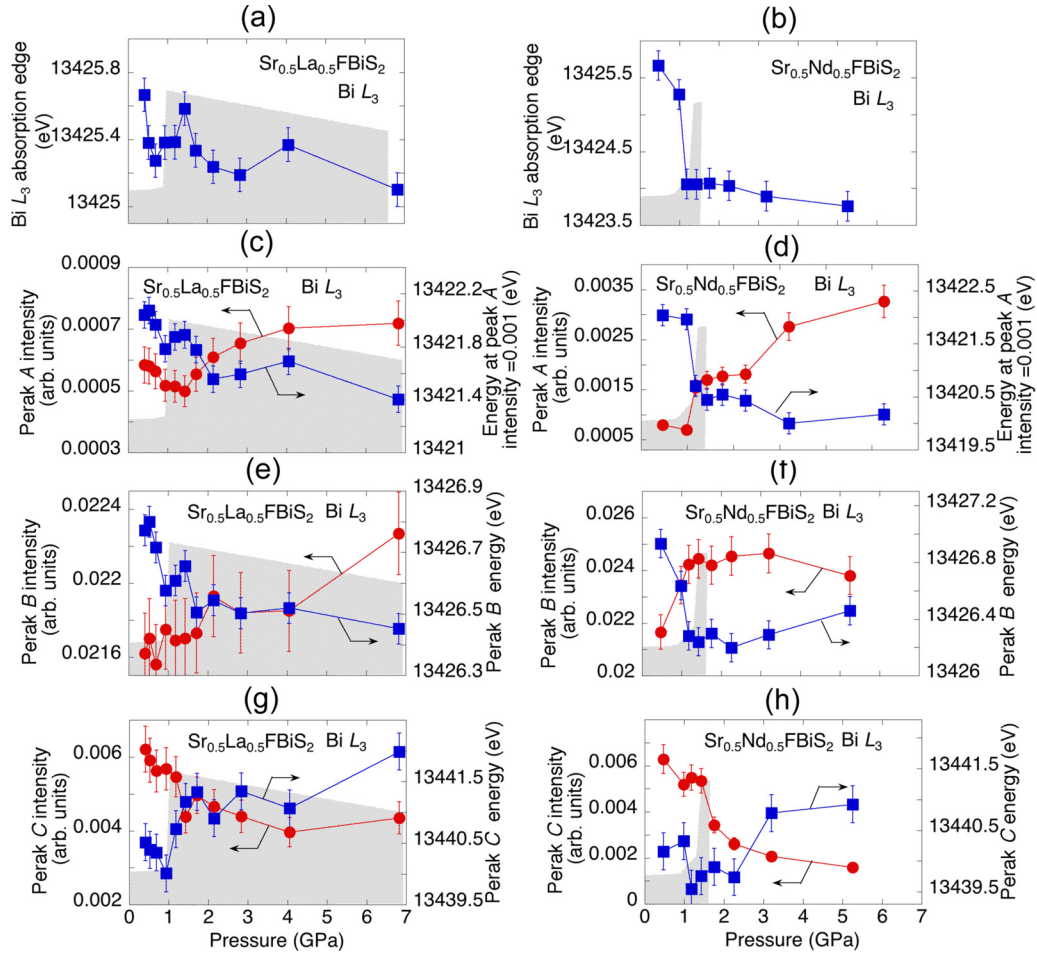


FIG. 5. Pressure dependence of the PFY-XAS spectra at the Bi- L_3 -absorption edge of (a) $\text{Sr}_{0.5}\text{La}_{0.5}\text{FBiS}_2$ and (b) $\text{Sr}_{0.5}\text{Nd}_{0.5}\text{FBiS}_2$. Pressure dependence of the intensity and energy of (c) the peak A, (e) the peak B, and (g) the peak C of $\text{Sr}_{0.5}\text{La}_{0.5}\text{FBiS}_2$. Pressure dependence of the intensity and energy of (d) the peak A, (f) the peak B, and (h) the peak C of $\text{Sr}_{0.5}\text{Nd}_{0.5}\text{FBiS}_2$. The shaded areas correspond to the superconducting regions where the maximum of the vertical axis is scaled to be 15 K.

s and d pDOS corresponds to the increase of the empty s and d states obtained from the results of the pressure dependence of the PFY-XAS spectra in Fig. 5. Total DOS at the Fermi level is estimated to be 2.4 states/eV for tetragonal structure and 1.6 states/eV for monoclinic structure. Note that we discuss the relation between the experimental PFY-XAS spectra and the calculated pDOS here. To validate this, we verified that a core hole, which is included in the final state of the XAS measurement while not considered in DOS calculation, has little effect on the difference of the XAS spectra between the tetragonal and monoclinic phases (see Fig. S7 in Ref. [54]).

The van Hove singularity locates at the Fermi level in the tetragonal phase and splits largely due to the decrease of the crystal symmetry in the monoclinic phase. This is the origin of the decrease of the total DOS at the Fermi level in the monoclinic phase. The shape of Bi s pDOS is similar to that of Bi p pDOS in the monoclinic phase as shown in Figs. 7(e) and 7(f). Therefore the increase of the Bi s pDOS in the monoclinic phase may be caused by the hybridization of the p and s orbitals due to the decrease of the Bi crystal field symmetry in the monoclinic phase. We verified that these features of DOS are kept unchanged even when one uses different methods

for dealing with $\text{Sr}_{0.5}\text{La}_{0.5}$ occupation in the calculation (see Fig. S5 in Ref. [54]).

IV. DISCUSSION

The pressure dependence of the angle β between the a and c axes in Fig. 3(e) increases with pressure in the monoclinic crystal structure phase keeping the high- T_c condition. This is in contrast to the chemical pressure effect in the tetragonal crystal structure phase. In the BiS_2 superconductors with the tetragonal structure at ambient pressure, both carrier doping and in-plane chemical pressure, which result in the system ideal tetragonal structure and suppress in-plane disorder, are required to induce the bulk superconductivity and the increase of T_c [5].

Pressure-induced changes in the electronic structures of $\text{Sr}_{0.5}\text{Nd}_{0.5}\text{FBiS}_2$ is more drastic compared to that of $\text{Sr}_{0.5}\text{La}_{0.5}\text{FBiS}_2$ around the pressure of the structural phase transition. Nd substitution causes a larger lattice shrinkage compared to La substitution, resulting in a larger in-plane chemical pressure. In practice, the lattice constant a for $\text{Sr}_{0.5}\text{Nd}_{0.5}\text{FBiS}_2$ is smaller than that for $\text{Sr}_{0.5}\text{La}_{0.5}\text{FBiS}_2$, which means the in-plane chemical pressure

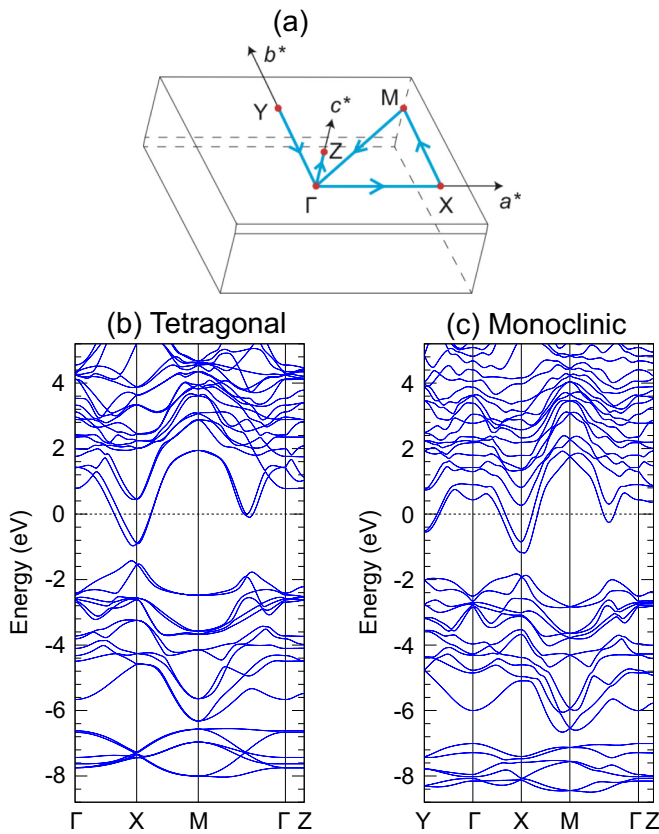


FIG. 6. (a) Brillouin zone in the monoclinic crystal structure. Band dispersion of $\text{Sr}_{0.5}\text{La}_{0.5}\text{FBiS}_2$ (b) in the tetragonal crystal structure (low pressure phase) and (c) in the monoclinic crystal structure (high-pressure, high- T_c phase). To compare these two band structures, we used the following names of k points for the monoclinic lattice while they are not conventional ones: $Y = (0, \pi/b, 0)$, $X = (\pi/a, 0, 0)$, $M = (\pi/a, \pi/b, 0)$, and $Z = (0, 0, \pi/c)$.

in $\text{Sr}_{0.5}\text{Nd}_{0.5}\text{FBiS}_2$ is larger than $\text{Sr}_{0.5}\text{La}_{0.5}\text{FBiS}_2$. Therefore local structural distortion is expected to be larger in $\text{Sr}_{0.5}\text{La}_{0.5}\text{FBiS}_2$. Since the La substitution is more unstable locally from a structural viewpoint, the phase transition probably begins partially and gradually earlier than in the case of the Nd substitution. T_c may be sensitive to the region where the monoclinic structure grows earlier. XRD measurements see the average structure and are insensitive to the above local change in the structure. Thus we could consider that the electronic structure measured through the partial fluorescence yield may be more sensitive to the pressure-induced local change. This could be understandable because we measure the partial electronic structure of Bi through the partial fluorescence yield measurements.

The x-ray spectroscopy study of $\text{Sr}_{0.5}\text{La}_{0.5}\text{FBiS}_2$ shows a large change in the electronic structure in the monoclinic crystal structure compared to that in the tetragonal crystal structure. The DFT calculations show that DOS of the s and d orbital increase just above E_F in the monoclinic crystal structure although the p DOS at E_F decreases. This explains the present spectroscopy results that the empty states of the Bi $6s$ and Bi $6d$ (t_{2g}) states increased in the monoclinic crystal structure.

In the tetragonal crystal structure before, the structural phase transition of $\text{Sr}_{1-x}\text{X}_x\text{FBiS}_2$ could be an unconventional superconductor and the superconductivity is filamentary like other BiS_2 -based compounds [20,22,23,61]. The shielding volume fraction of the superconductivity increases with pressure in the tetragonal phase, but the structural phase transition occurs before obtaining the complete bulk superconductivity. It seems that the phase transition occurs inevitably for the complete bulk superconductivity. On the other hand, the monoclinic crystal structure of $\text{Sr}_{1-x}\text{X}_x\text{FBiS}_2$ after the structural transition the superconductivity is considered to be a phonon-mediated conventional [20]. We suppose that similar things happens also in $\text{XO}_{1-x}\text{F}_x\text{BiS}_2$. Thus, in $\text{Sr}_{1-x}\text{X}_x\text{FBiS}_2$, the mechanism of the superconductivity is different between the two phases of the tetragonal and monoclinic crystal structures and this may be in common in the BiS_2 based superconductors. In the phonon-mediated superconductors, T_c has been estimated using McMillan-Allen-Dynes formula [62,63]. In $\text{LaO}_{0.5}\text{F}_{0.5}\text{BiS}_2$, the electron-phonon coupling constant λ was estimated to be 0.6–0.85 [64–66] and T_c was reduced to be on the order of 10 K for the screened Coulomb interaction parameter $\mu^* = 0.1$. Therefore, if the value of λ in $\text{Sr}_{1-x}\text{X}_x\text{FBiS}_2$ is the same order as that in $\text{LaO}_{0.5}\text{F}_{0.5}\text{BiS}_2$, high T_c could be explained as the phonon-mediated superconductor.

In superconductors, in general, the emergence of the superconductivity or the increase of T_c occurs when DOS at the Fermi level (E_F) increases. For example, in the tetragonal phase of LaOBiS_2 , the electron doping by the substitution of F to the O site caused the increase of DOS at E_F , resulting in the increase of T_c [66]. In Bi_2Se_3 , the pressure-induced structural transition induced the emergency of the superconductivity accompanying the rapid increase of DOS at E_F [32,67]. On the other hand, in $\text{Sr}_{1-x}\text{X}_x\text{FBiS}_2$ DOS at E_F in the high-pressure phase did not show a significant change. Here, however, we should note that the mechanism to emerge the superconductivity in the high-pressure phase is different from that in the low-pressure phase as described above. The different mechanisms of the superconductivity between two phases could be a main reason why DOS at E_F did not increase even if T_c increased and why high T_c was kept even if the deviation from the tetragonal structure was larger with pressure in the high-pressure phase.

Additionally, we note the importance of the in-plane disorder in the BiS_2 network. In $\text{LaO}_{0.5}\text{F}_{0.5}\text{BiS}_{2-x}\text{Se}_x$, the increase of the Se content induced the reduction of in-plane disorder in the BiS_2 network with being the system more metallic and enhancing the superconductivity in the tetragonal phase [68,69]. The pressure effect on the in-plane disorder is not known and the present DFT calculations do not include such in-plane disorder.

The temperature dependence of the resistivity seems to show the transition from semiconductor at the low-pressure phase to metal at the high-pressure phase. In the DFT calculations, we did not observe a significant increase of DOS at the Fermi level. We consider that this is caused by the following reasons. (i) In the tetragonal structure at low pressure the symmetry of the crystal structure is broken locally. At this time, the temperature dependence of the electrical resistance becomes semiconductor-like due to carrier localization [69].

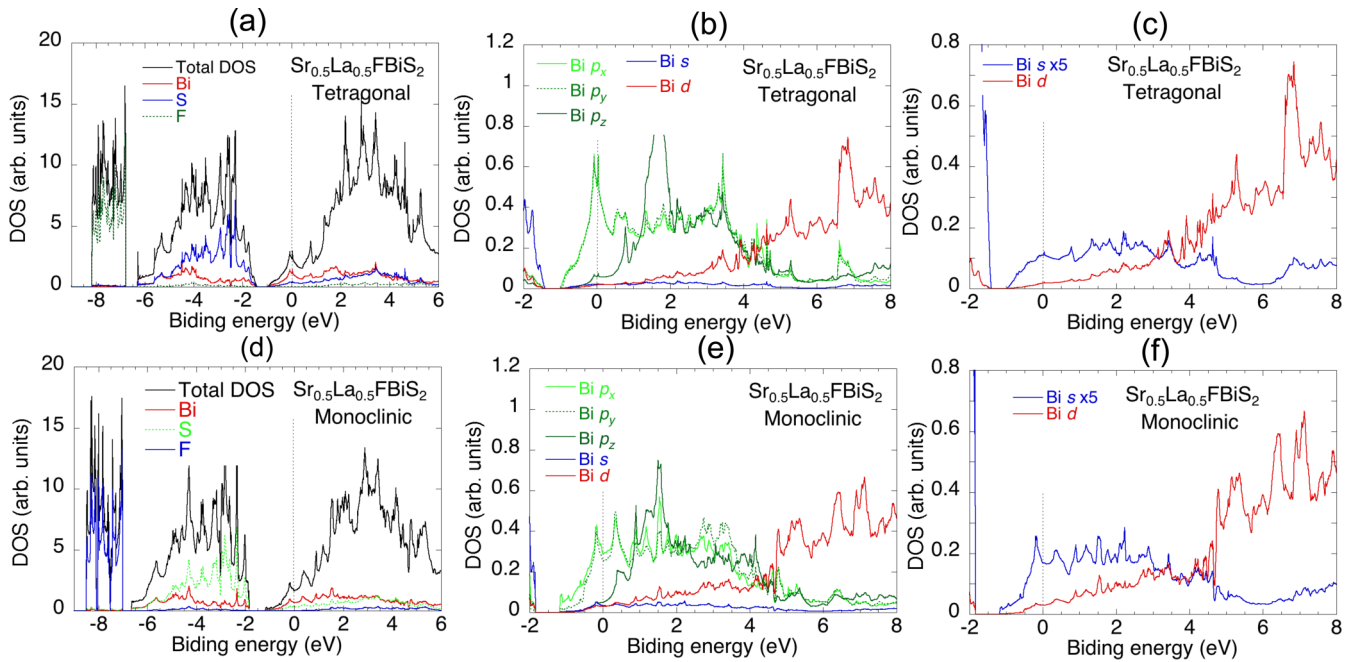


FIG. 7. Total and partial DOS in the tetragonal crystal structure [(a)–(c)] and in the monoclinic crystal structure [(d)–(f)]. Note that in (c) and (f) DOS of Bi *s* is multiplied by a factor of 5. Total DOS at the Fermi level is estimated to be 2.4 states/eV for the tetragonal structure and 1.6 states/eV for the monoclinic structure.

In this state, superconductivity goes from filamentary to bulk with pressure. (ii) In the monoclinic structure at high pressure, it is known that various BiS₂-based systems become metallic. Therefore the local turbulence in the tetragonal structure has gone (or is very weak) in the monoclinic structure. The cause of the local structural disturbance of the tetragonal crystal is considered to be the structural instability due to the Bi lone pair [70]. In the monoclinic crystal with reduced in-plane symmetry, the lone pair's location is probably fixed and structurally the system becomes stable. On the other hand, it is difficult for DFT calculation to incorporate such local structural disorder and its effect on the transport property as described above. Therefore our DFT calculation cannot reproduce the semiconductor-to-metal transition at low pressure. A study of the in-plane disorder effect under pressure as well as the theoretical calculation of T_c in the high-pressure phase remains to challenge in the future.

V. CONCLUSION

The XRD study of Sr_{0.5}La_{0.5}FBiS₂ and Sr_{0.5}Nd_{0.5}FBiS₂ under pressure was performed and the monoclinic crystal structure ($P2_1/m$) in the high-pressure phase was clarified. In Sr_{0.5}La_{0.5}FBiS₂ the structural transition occurred before reaching to the critical in-plane color red chemical pressure to increase T_c in the tetragonal crystal structure.

We extend the measurement of T_c for Sr_{0.5}La_{0.5}FBiS₂ up to 6.5 GPa. The result showed a gradual decrease of T_c in the monoclinic crystal structure.

The XAS study of Sr_{1-x}X_xFBiS₂ was performed systematically. Pressure-induced changes in the electronic structures of Sr_{0.5}Nd_{0.5}FBiS₂ were drastic around the pressure of the structural phase transition. On the other hand, that of

Sr_{0.5}La_{0.5}FBiS₂ changed continuously. The results suggest that the PFY-XAS measurements are more sensitive to the local distortion of the crystal structure compared to XRD. In Sr_{0.5}La_{0.5}FBiS₂ and Sr_{0.5}Nd_{0.5}FBiS₂, the energy of the Bi-*L*₃ absorption edge decreased around the structural transition pressure. This correlated to the transition from a semiconductorlike to more metallic states. Pressure the empty states of Bi *s* and *d* (t_{2g}) bands above the Fermi level in the high-pressure phase. This corresponds to the DFT results that DOS of the *s* and *d* orbital increase just above E_F in the monoclinic crystal structure.

The DFT calculations showed an unusual phenomenon that a slight decrease of DOS at E_F was shown even in the high- T_c phase. This may be caused by the fact that the DFT calculations could not incorporate local structure in the tetragonal structure and thus did not reproduce the electronic states at low pressure properly.

ACKNOWLEDGMENTS

The experiments were performed at SPring-8 Taiwan beamline BL12XU and BL12B2 under SPring-8 Proposals No. 2019B4269, No. 2020A4269, No. 2021A4253, and No. 2021B4254, corresponding NSRRC Proposals No. 2019-2-030, No. 2019-2-265, No. 2019-3-004, 2021-1-009, and No. 2021-1-415. This work has been partly supported by Grants-in-Aid for Scientific Research (KAKENHI 18K18743, 18KK0076, 21K18834, 21K03442, 21H00151, and 22K04908) from MEXT, Japan, and by the Program for Promoting the Enhancement of Research Universities, and Tokyo Metropolitan Government Advanced Research (H31-1).

- [1] Y. Mizuguchi, H. Fujihisa, Y. Gotoh, K. Suzuki, H. Usui, K. Kuroki, S. Demura, Y. Takano, H. Izawa, and O. Miura, BiS₂-based layered superconductor Bi₄O₄S₃, *Phys. Rev. B* **86**, 220510(R) (2012).
- [2] Y. Mizuguchi, S. Demura, K. Deguchi, Y. Takano, H. Fujihisa, Y. Gotoh, H. Izawa, and O. Miura, Superconductivity in novel BiS₂-based layered superconductor LaO_{1-x}F_xBiS₂, *J. Phys. Soc. Jpn.* **81**, 114725 (2012).
- [3] J. Xing, S. Li, X. Ding, H. Yang, and H.-H. Wen, Superconductivity appears in the vicinity of semiconducting-like behavior in CeO_{1-x}F_xBiS₂, *Phys. Rev. B* **86**, 214518 (2012).
- [4] S. K. Singh, A. Kumar, B. Gahtori, Shruti, G. Sharma, S. Patnaik, and V. P. S. Awana, Bulk Superconductivity in Bismuth Oxysulfide Bi₄O₄S₃, *J. Am. Chem. Soc.* **134**, 16504 (2012).
- [5] Y. Mizuguchi, Material development and physical properties of BiS₂-based layered compounds, *J. Phys. Soc. Jpn.* **88**, 041001 (2019).
- [6] K. Hoshi and Y. Mizuguchi, Experimental overview on pairing mechanisms of BiCh₂-based (Ch: S, Se) layered superconductors, *J. Phys.: Condens. Matter* **33**, 473001 (2021).
- [7] S. Demura, Y. Mizuguchi, K. Deguchi, H. Okazaki, H. Hara, T. Watanabe, S. J. Denholme, M. Fujioka, T. Ozaki, H. Fujihisa, Y. Gotoh, O. Miura, T. Yamaguchi, H. Takeya, and Y. Takano, New member of BiS₂-based superconductor NdO_{1-x}F_xBiS₂, *J. Phys. Soc. Jpn.* **82**, 033708 (2013).
- [8] R. Jha, A. Kumar, S. K. Singh, and V. P. S. Awana, Synthesis and superconductivity of new BiS₂ based superconductor PrO_{0.5}F_{0.5}BiS₂, *J. Supercond. Nov. Magn.* **26**, 499 (2013).
- [9] Y. Goto, R. Sogabe, and Y. Mizuguchi, Bulk superconductivity induced by Se substitution in BiCh₂-based layered compounds Eu_{0.5}Ce_{0.5}F_xBiS_{2-x}Se_x, *J. Phys. Soc. Jpn.* **86**, 104712 (2017).
- [10] R. Jha, B. Tiwari, and V. P. S. Awana, Impact of hydrostatic pressure on superconductivity of Sr_{0.5}La_{0.5}F_xBiS₂, *J. Phys. Soc. Jpn.* **83**, 063707 (2014).
- [11] R. Jha, B. Tiwari, and V. P. S. Awana, Appearance of bulk superconductivity under hydrostatic pressure in Sr_{0.5}RE_{0.5}F_xBiS₂ (RE = Ce, Nd, Pr, and Sm) compounds, *J. Appl. Phys.* **117**, 013901 (2015).
- [12] R. Jha and V. P. S. Awana, Effect of hydrostatic pressure on BiS₂-based layered superconductors: A review, *Nov. Supercond. Mater.* **2**, 16 (2016).
- [13] H. Koteagwa, Y. Tomita, H. Tou, H. Izawa, Y. Mizuguchi, O. Miura, S. Demura, K. Deguchi, and Y. Takano, Pressure study of BiS₂-based superconductors Bi₄O₄S₃ and La(O, F)BiS₂, *J. Phys. Soc. Jpn.* **81**, 103702 (2012).
- [14] C. T. Wolowiec, D. Yazici, B. D. White, K. Huang, and M. B. Maple, Pressure-induced enhancement of superconductivity and suppression of semiconducting behavior in LnO_{0.5}F_{0.5}BiS₂ (Ln = La, Ce) compounds, *Phys. Rev. B* **88**, 064503 (2013).
- [15] T. Tomita, M. Ebata, H. Soeda, H. Takahashi, H. Fujihisa, Y. Gotoh, Y. Mizuguchi, H. Izawa, O. Miura, S. Demura, K. Deguchi, and Y. Takano, Pressure-induced enhancement of superconductivity and structural transition in BiS₂-layered LaO_{1-x}F_xBiS₂, *J. Phys. Soc. Jpn.* **83**, 063704 (2014).
- [16] V. Svitlyk, A. Krzton-Maziopa, and M. Mezouar, Pressure-induced enhancement of two-dimensionality in LaO_{1-x}F_xBi(S/Se)₂ superconductors, *Phys. Rev. B* **100**, 144107 (2019).
- [17] L. Li, Y. Li, Y. Jin, H. Huang, B. Chen, X. Xu, J. Dai, L. Zhang, X. Yang, H. Zhai, G. Cao, and Z. Xu, Co-existence of superconductivity and ferromagnetism in Sr_{0.5}Ce_{0.5}F_xBiS₂, *Phys. Rev. B* **91**, 014508 (2015).
- [18] W. You, L. Li, H. Y. Yang, J.-L. Wang, H. Y. Mao, L. Zhang, C. Y. Xi, J. Cheng, Y. K. Luo, J. H. Dai, and Y. K. Li, Superconductivity, electronic phase diagram, and pressure effect in Sr_{1-x}Pr_xF_xBiS₂, *Sci. China: Phys. Mech. Astron.* **62**, 957411 (2019).
- [19] A. Laref, R. M. Al-Amer, Z. A. Alahmed, S. Laref, I. Islam, S. A. Khandy, Y. C. Xiong, H. M. Huang, and X. Wu, Electronic structure and optical anisotropy in Sr_{1-x}Ba_xF_xBiS₂ (x = 0, 0.25, 0.5, 0.75, 1) based solar cell materials, *Res. Phys.* **16**, 102808 (2020).
- [20] A. Yamashita, R. Jha, Y. Goto, A. Miura, C. Moriyoshi, Y. Kuroiwa, C. Kawashima, K. Ishida, H. Takahashi, and Y. Mizuguchi, Evolution of two bulk-superconducting phases in Sr_{0.5}RE_{0.5}F_xBiS₂ (RE: La, Ce, Pr, Nd, Sm) by external hydrostatic pressure effect, *Sci. Rep.* **10**, 12880 (2020).
- [21] A. Yamashita, H. Usui, K. Hoshi, Y. Goto, K. Kuroki, and Y. Mizuguchi, Possible pairing mechanism switching driven by structural symmetry breaking in BiS₂-based layered superconductors, *Sci. Rep.* **11**, 230 (2021).
- [22] K. Hoshi, Y. Goto, and Y. Mizuguchi, Selenium isotope effect in the layered bismuth chalcogenide superconductor LaO_{0.6}F_{0.4}Bi(S, Se)₂, *Phys. Rev. B* **97**, 094509 (2018).
- [23] R. Jha and Y. Mizuguchi, Unconventional isotope effect on transition temperature in BiS₂-based superconductor Bi₄O₄S₃, *Appl. Phys. Express* **13**, 093001 (2020).
- [24] T. Machida, Y. Fujisawa, M. Nagao, S. Demura, K. Deguchi, Y. Mizuguchi, Y. Takano, and H. Sakata, Checkerboard stripe electronic state on cleaved surface of NdO_{0.7}F_{0.3}BiS₂ probed by scanning tunneling microscopy, *J. Phys. Soc. Jpn.* **83**, 113701 (2014).
- [25] K. Suzuki, H. Usui, K. Kuroki, and H. Ikeda, Charge and quadrupole fluctuations and gap anisotropy in BiS₂-based superconductors, *Phys. Rev. B* **96**, 024513 (2017).
- [26] K. Suzuki, H. Usui, K. Kuroki, T. Nomoto, K. Hattori, and H. Ikeda, Electronic structure and superconducting gap structure in BiS₂-based layered superconductors, *J. Phys. Soc. Jpn.* **88**, 041008 (2019).
- [27] P. Dong, J. Cheng, and Y. Li, Role of local atomic displacements in the superconductivity of Sr_{0.5}La_{0.5}F_xBiS₂ and Sr_{0.5}La_{0.5}F_xBiSe₂ system, *Mater. Res. Bull.* **111**, 154 (2019).
- [28] K. Hämäläinen, D. P. Siddons, J. B. Hastings, and L. E. Berman, Elimination of the Inner-Shell Lifetime Broadening in X-ray-Absorption Spectroscopy, *Phys. Rev. Lett.* **67**, 2850 (1991).
- [29] K. Hämäläinen, C. C. Kao, J. B. Hasting, D. P. Siddons, L. E. Berman, V. Stojanoff, and S. P. Cramer, Spin-dependent x-ray absorption of MnO and MnF₂, *Phys. Rev. B* **46**, 14274 (1992).
- [30] J.-P. Rueff and A. Shukla, Inelastic x-ray scattering by electronic excitations under high pressure, *Rev. Mod. Phys.* **82**, 847 (2010).
- [31] H. Yamaoka, Pressure dependence of the electronic structure of 4f and 3d electron systems studied by x-ray emission spectroscopy, *High Press. Res.* **36**, 262 (2016).
- [32] H. Yamaoka, H. O. Jeschke, X. Yang, T. He, H. Goto, N. Hiraoka, H. Ishii, J. Mizuki, and Y. Kubozono, Electronic structures of Bi₂Se₃ and Ag_xBi₂Se₃ under pressure studied by high-resolution x-ray absorption spectroscopy and density functional theory calculations, *Phys. Rev. B* **102**, 155118 (2020).

- [33] K. Kitagawa, H. Gotou, T. Yagi, A. Yamada, T. Matsumoto, Y. Uwatoko, and M. Takigawa, Space efficient opposed-anvil high-pressure cell and its application to optical and NMR measurements up to 9 GPa, *J. Phys. Soc. Jpn.* **79**, 024001 (2010).
- [34] A. P. Hammersley, S. O. Svensson, M. Hanfland, A. N. Fitch, and D. Häusermann, Two-dimensional detector software: From real detector to idealised image or two-theta scan, *High Press. Res.* **14**, 235 (1996).
- [35] K. Momma and F. Izumi, VESTA: A three-dimensional visualization system for electronic and structural analysis, *J. Appl. Crystallogr.* **41**, 653 (2008).
- [36] F. Izumi and K. Momma, Three-dimensional visualization in powder diffraction, *Solid State Phenom.* **130**, 15 (2007).
- [37] K. Momma and F. Izumi, VESTA 3 for three-dimensional visualization of crystal, volumetric and morphology data, *J. Appl. Crystallogr.* **44**, 1272 (2011).
- [38] H. Yamaoka, Y. Yamamoto, E. F. Schwier, N. Tsujii, M. Yoshida, Y. Ohta, H. Sakurai, J.-F. Lin, N. Hiraoka, H. Ishii, K.-D. Tsuei, M. Arita, K. Shimada, and J. Mizuki, Pressure-induced phase transition in LaCo_5 studied by x-ray emission spectroscopy, x-ray diffraction and density functional theory, *Phys. Rev. B* **94**, 165156 (2016).
- [39] H. Yamaoka, Y. Yamamoto, J.-F. Lin, Junjie J. Wu, X. Wang, C. Jin, M. Yoshida, S. Onari, S. Ishida, Y. Tsuchiya, N. Takeshita, N. Hiraoka, H. Ishii, K.-D. Tsuei, P. Chow, Y. Xiao, and J. Mizuki, Electronic structures and spin states of BaFe_2As_2 and SrFe_2As_2 probed by x-ray emission spectroscopy at Fe and As K-absorption edges, *Phys. Rev. B* **96**, 085129 (2017).
- [40] H.-K. Mao and P. M. Bell, High-pressure physics: The 1-megabar mark on the ruby $R1$ static pressure scale, *Science* **191**, 851 (1976).
- [41] K. Syassen, Ruby under Pressure, *High Press. Res.* **28**, 75 (2008).
- [42] H. Yamaoka, Y. Zekko, I. Jarrige, J.-F. Lin, N. Hiraoka, H. Ishii, K.-D. Tsuei, and J. Mizuki, Ruby pressure scale in a low-temperature diamond anvil cell, *J. Appl. Phys.* **112**, 124503 (2012).
- [43] J. P. Perdew, K. Burke, and M. Ernzerhof, Generalized Gradient Approximation Made Simple, *Phys. Rev. Lett.* **77**, 3865 (1996).
- [44] G. Kresse and D. Joubert, From ultrasoft pseudopotentials to the projector augmented-wave method, *Phys. Rev. B* **59**, 1758 (1999).
- [45] G. Kresse and J. Hafner, Ab initio molecular dynamics for liquid metals, *Phys. Rev. B* **47**, 558(R) (1993).
- [46] G. Kresse and J. Hafner, Ab initio molecular-dynamics simulation of the liquid-metal-amorphous-semiconductor transition in germanium, *Phys. Rev. B* **49**, 14251 (1994).
- [47] G. Kresse and J. Furthmüller, Efficiency of ab-initio total energy calculations for metals and semiconductors using a plane-wave basis set, *Comput. Mater. Sci.* **6**, 15 (1996).
- [48] G. Kresse and J. Furthmüller, Efficient iterative schemes for ab initio total-energy calculations using a plane-wave basis set, *Phys. Rev. B* **54**, 11169 (1996).
- [49] B. Joseph, A. Iadecola, L. Simonelli, Y. Mizuguchi, Y. Takano, T. Mizokawa, and N. L. Saini, A study of the electronic structure of $\text{FeSe}_{1-x}\text{Te}_x$ chalcogenides by Fe and Se K -edge x-ray absorption near edge structure measurements, *J. Phys.: Condens. Matter* **22**, 485702 (2010).
- [50] C. L. Chen, S. M. Rao, C. L. Dong, J. L. Chen, T. W. Huang, B. H. Mok, M. C. Ling, W. C. Wang, C. L. Chang, and T. S. Chan, X-ray absorption spectroscopy investigation of the electronic structure of superconducting FeSe_x single crystals, *Europhys. Lett.* **93**, 47003 (2011).
- [51] N. L. Saini, T. Mizokawa, E. Magnano, S. Nappini, F. Bondino, H. Takeya, Y. Mizuguchi, Y. Takano, and K. B. Garg X-ray absorption and photoemission spectroscopy of electronic phase separation in $\text{K}_x\text{Fe}_{2-y}\text{Se}_2$, *Phys. Rev. B* **90**, 184510 (2014).
- [52] A. I. Figueroa, G. van der Laan, Liam J. Collins-McIntyre, G. Cibin, A. J. Dent, and T. Hesjedal, Local structure and bonding of transition metal dopants in Bi_2Se_3 topological insulator thin films, *J. Phys. Chem.* **119**, 17344 (2015).
- [53] A. A. Rahman, R. Huang, and L. Whittaker-Brooks, Distinctive extrinsic atom effects on the structural, optical, and electronic properties of $\text{Bi}_2\text{S}_{3-x}\text{Se}_x$ solid solutions, *Chem. Mater.* **28**, 6544 (2016).
- [54] See Supplemental Material at <http://link.aps.org/supplemental/10.1103/PhysRevB.106.205122> for (i) The analyses of the PFY-XAS spectra with a different normalization method. (ii) The detailed results of the analyses of the XRD patterns in the high-pressure phase of $\text{Sr}_{0.5}\text{La}_{0.5}\text{FBiS}_2$: a fit example of the XRD patterns, atomic coordinations, and atomic distances. We also show the XRD patterns of $\text{Sr}_{0.5}\text{Nd}_{0.5}\text{FBiS}_2$ with the analyzed results. (iii) Comparison of DOS calculated under several conditions, calculated XAS spectra, which includes Refs. [71,72].
- [55] Y. Mizuguchi, A. Miura, J. Kajitani, T. Hiroi, O. Miura, K. Tadanaga, N. Kumada, E. Magome, C. Moriyoshi, and Y. Kuroiwa, In-plane chemical pressure essential for superconductivity in BiCh_2 -based (Ch : S, Se) layered structure, *Sci. Rep.* **5**, 14968 (2015).
- [56] S. M. Heald, D. DiMarzio, M. Croft, M. S. Hegde, S. Li, and M. Greenblatt, X-ray-absorption study of charge-density ordering in $(\text{Ba}_{1-x}\text{K}_x)\text{BiO}_3$, *Phys. Rev. B* **40**, 8828 (1989).
- [57] R. Retoux, F. Studer, C. Michel, B. Raveau, A. Fontaine, and E. Dartyge, Valence state for bismuth in the superconducting bismuth cuprates, *Phys. Rev. B* **41**, 193 (1990).
- [58] A. N. Baranov, J. S. Kim, D. C. Kim, D. S. Suh, Y. W. Park, and E. V. Antipov, X-ray absorption near-edge structure spectra study of the $\text{Ba}_{1-x}\text{K}_x\text{BiO}_3$ ($0.37 \leq x \leq 1.0$) superconductor, *Physica C* **383**, 95 (2002).
- [59] M. Ochi, R. Akashi, and K. Kuroki, Strong bilayer coupling induced by the symmetry breaking in the monoclinic phase of BiS_2 -based superconductors, *J. Phys. Soc. Jpn.* **85**, 094705 (2016).
- [60] H. Usui, K. Suzuki, and K. Kuroki, Minimal electronic models for superconducting BiS_2 layers, *Phys. Rev. B* **86**, 220501(R) (2012).
- [61] Y. Ota, K. Okazaki, H. Q. Yamamoto, T. Yamamoto, S. Watanabe, C. Chen, M. Nagao, S. Watauchi, I. Tanaka, Y. Takano, and S. Shin, Unconventional Superconductivity in the BiS_2 -Based Layered Superconductor $\text{Nd}_{0.71}\text{F}_{0.29}\text{BiS}_2$, *Phys. Rev. Lett.* **118**, 167002 (2017).
- [62] W. L. McMillan, Transition temperature of strong-coupled superconductors, *Phys. Rev.* **167**, 331 (1968).
- [63] P. B. Allen and R. C. Dynes, Transition temperature of strong-coupled superconductors reanalyzed, *Phys. Rev. B* **12**, 905 (1975).
- [64] X. Wan, H.-C. Ding, S. Y. Savrasov, and C.-G. Duan, Electron-phonon superconductivity near charge-density-wave instability

- in $\text{LaO}_{0.5}\text{F}_{0.5}\text{BiS}_2$: Density-functional calculations, *Phys. Rev. B* **87**, 115124 (2013).
- [65] B. Li, Z. W. Xing, and G. Q. Huang, Phonon spectra and superconductivity of the BiS_2 -based compounds $\text{LaO}_{1-x}\text{F}_x\text{BiS}_2$, *Europhys. Lett.* **101**, 47002 (2013).
- [66] T. Yildirim, Ferroelectric soft phonons, charge density wave instability, and strong electron-phonon coupling in BiS_2 layered superconductors: A first-principles study, *Phys. Rev. B* **87**, 020506(R) (2013).
- [67] T. He, X. F. Yang, T. Terao, T. Uchiyama, T. Ueno, K. Kobayashi, J. Akimitsu, T. Miyazaki, T. Nishioka, K. Kimura, K. Hayashi, N. Happono, H. Yamaoka, H. Ishii, Y.-F. Liao, H. Ota, and Y. Kubozono, Pressure-induced superconductivity in $\text{Ag}_x\text{B}_{2-x}\text{Se}_3$, *Phys. Rev. B* **97**, 104503 (2018).
- [68] E. Paris, Y. Mizuguchi, M. Y. Hacisalihoglu, T. Hiroi, B. Joseph, G. Aquilanti, O. Miura, T. Mizokawa, and N. L. Saini, Role of the local structure in superconductivity of $\text{LaO}_{0.5}\text{F}_{0.5}\text{BiS}_{2-x}\text{Se}_x$ system, *J. Phys.: Condens. Matter* **29**, 145603 (2017).
- [69] Y. Yuan, H. Arima, M. Masaoka, Y. Naito, Y. Hijikata, R. Jha, Y. Mizuguchi, and K. Matsubayashi, Pressure tuning of localization and superconductivity in LaOPbBiS_3 and $\text{La}_2\text{O}_2\text{Bi}_3\text{AgS}_6$, *Phys. Rev. B* **105**, 064509 (2022).
- [70] Y. Mizuguchi, E. Paris, T. Sugimoto, A. Iadecola, J. Kajitani, O. Miura, T. Mizokawa, and N. L. Saini, The effect of *RE* substitution in layered $\text{REO}_{0.5}\text{F}_{0.5}\text{BiS}_2$: Chemical pressure, local disorder and superconductivity, *Phys. Chem. Chem. Phys.* **17**, 22090 (2015).
- [71] P. Blaha, K. Schwarz, G. K. H. Madsen, D. Kvasnicka, J. Luitz, R. Laskowski, F. Tran, and L. D. Marks, WIEN2k, An Augmented Plane Wave + Local Orbitals Program for Calculating Crystal Properties (Karlheinz Schwarz, Vienna University of Technology, Austria, 2018).
- [72] P. Blaha, K. Schwarz, F. Tran, R. Laskowski, G. K. H. Madsen, and L. D. Marks, WIEN2k: An APW+lo program for calculating the properties of solids, *J. Chem. Phys.* **152**, 074101 (2020).